energies

MDPI

Article

Optimization of Well Configurations and Production–Injection Parameters in Sandstone Geothermal Reservoirs Using Thermo-Hydro-Mechanical Coupled Modeling

Mingzhu Wang [1,2,3], Xi Yang [4], Yabin Yang [1,2,3], Qing Sha [5,*], Yaqi Zhao [4] and Pengpeng Ding [4]

[1] The Second Institute of Hydrogeology and Engineering Geology, Shandong Provincial Bureau of Geology & Mineral Resources (Lubei Geo-Engineering Exploration Institute of ShandongProvince), Dezhou 253072, China; 18853184768@163.com (M.W.)
[2] Shandong Provincial Research Center of Geothermal Resources and Reinjection, Dezhou 253072, China
[3] Dezhou Deep Geological Energy Conservation and Carbon Reduction Key Laboratory, Dezhou 253072, China
[4] School of Civil and Hydraulic Engineering, Ningxia University, Yinchuan 750021, China
[5] Shandong Provincial Lunan Geology and Exploration Institute (Shandong Provincial Bureau of Geology and Mineral Resources No.2 Geological Brigade), Jining 272100, China
* Correspondence: 17860725026@163.com; Tel.: +86-17860725026

Abstract

Optimizing well spacing, well configurations and production–injection parameters is crucial for maintaining the hydraulic and thermal performance of sandstone geothermal reservoirs during long-term exploitation. This study develops a three-dimensional thermo-hydro-mechanical (THM) coupled numerical model of a sandstone geothermal reservoir in Linqing City, China, to investigate the effects of well arrangements and operating conditions on reservoir performance. The influences of well spacing and 14 multi-well configurations on groundwater drawdown and production temperature are systematically evaluated over a 30-year operation period. In addition, a three-factor, three-level orthogonal experimental design, combined with range analysis and analysis of variance, is employed to identify the dominant operating parameters governing reservoir responses. The results reveal a trade-off between groundwater drawdown and thermal interference when determining well spacing. A well spacing of 400 m provides a favorable balance, resulting in a groundwater drawdown of approximately 0.5 m and a production temperature decline of only 0.34 °C after 30 years. For multi-well systems, the linear configuration (Pattern II) exhibits the most favorable overall performance in both two-injection–one-production and one-injection–two-production arrangements, whereas the diamond-shaped configuration (Pattern IV) minimizes groundwater drawdown to 0.11 m in the two-injection–two-production system. Sensitivity analysis further indicates that the injection ratio is the dominant factor influencing groundwater drawdown ($p = 0.035$), while the production rate exerts the greatest influence on production temperature ($p = 0.047$). These findings highlight the importance of coordinating well configurations and operating parameters to mitigate hydraulic and thermal interference, providing practical guidance for the sustainable development and long-term management of sandstone geothermal reservoirs.

Keywords: geothermal energy; numerical model; well spacing; well network; production–injection optimization

Check for updates

Academic Editor: Massimo Dentice D'Accadia

Received: 28 October 2026
Revised: 24 November 2026
Accepted: 25 November 2026
Published: 29 November 2026

Copyright: © 2026 by the authors. Licensee MDPI, Basel, Switzerland. This article is an open access article distributed under the terms and conditions of the Creative Commons Attribution (CC BY) license.

1. Introduction

With the global urgency of energy transformation and carbon neutrality, geothermal energy has become a key renewable energy source because of its inherent advantages such

https://doi.org/10.3390/en19235779

as clean and low carbon [1,2]. The rapid development of renewable green energy has become a global consensus [3,4]. Under this background, optimizing the thermal reservoir production injection mode is the key premise to realize its sustainable development [5,6]. However, as an important carrier of geothermal development, porous thermal storage such as sandstone is restricted by technical problems such as low injectivity and uneven interlayer injection [7–9].

At present, the research methods of thermal storage production injection optimization mainly include analytical method, model test and numerical simulation [10,11]. Although the model test can obtain intuitive test data, there are great limitations in adjusting the production and injection scheme [12,13]. The numerical simulation method is to establish a multi-field coupled numerical model of thermal reservoir, adjust key parameters such as geothermal well spacing or production and injection scheme, optimize the production and injection mode of thermal storage, and provide technical support for the sustainable management of geothermal system [14,15].

Nowadays, numerical simulation has been widely applied to the optimization of geothermal well spacing and production schemes. For example, TOUGH2 was used to simulate the thermal reservoir in Tianjin Binhai New Area, and the influence of injection conditions on the pressure and temperature fields was analyzed [16]. A well group model was established in western Turkey through monitoring and analysis, and the optimal production scheme was determined according to variations in reservoir pressure [17]. A three-dimensional fluid–solid coupling model was developed to analyze the dynamic effects of injection rate and well spacing on carbonate geothermal reservoirs [18,19]. By combining a data-driven geothermal power plant model, a comprehensive evaluation was conducted using a thermodynamic flow table model, and an optimization scheme was proposed [20,21].

Numerical modeling has been widely used to evaluate the effects of well layout on geothermal reservoir performance. Thermal responses under different well arrangements were investigated in [22], and geothermal heat-recovery optimization in the West Netherlands Basin was examined in [23]. A cluster-layout well pattern for the Dezhou geothermal field was investigated in [24]. These studies establish the importance of well geometry, but their layout recommendations must be interpreted in relation to reservoir characteristics and operating conditions. The productivity potential of a granite-type enhanced geothermal system was examined in [25], whereas a five-spot horizontal-well system was investigated in [26] using thermal–fluid–solid coupling. Their geological settings and well geometries differ from those of the sandstone reservoir considered here. For the Podhale geothermal system, more than 20 years of stable operation was reported in [27], with production exceeding 500 m^3/h at a wellhead temperature of 86 °C and only a small pressure decline and negligible temperature change. These findings demonstrate the potential for sustained geothermal production but do not establish a directly transferable well-layout recommendation for the Linqing sandstone reservoir. The question addressed in the present study is therefore how well spacing and multi-well configuration balance groundwater drawdown against production-temperature decline under the same modeled geological and operating conditions.

Beyond well spacing and well configurations, operating parameters also influence the long-term hydraulic and thermal performance of geothermal reservoirs. Previous studies have demonstrated that production and injection conditions affect reservoir pressure evolution, thermal breakthrough and production temperature. For example, studies of sandstone geothermal reservoirs have quantified the effects of injection temperature, flow rate and well spacing on thermal breakthrough [28]. Sbai and Larabi [29] identified production flow rate as an important factor affecting geothermal doublet performance, while Suilmann

et al. [30] evaluated the combined effects of well spacing, production rate and reinjection temperature on production temperature and doublet lifetime. These findings demonstrate the importance of operating conditions in geothermal development. However, the relative effects of production rate, injection ratio and injection temperature on groundwater drawdown and production temperature remain insufficiently quantified for the sandstone geothermal reservoir considered in this study.

Previous studies have investigated the effects of well arrangements and operating conditions on geothermal reservoir performance. However, their findings are conditioned by reservoir characteristics, well-completion conditions and operating assumptions, which limits their direct transfer to the Linqing sandstone reservoir. The question addressed here is which well spacings and configurations provide a favorable balance between groundwater drawdown and production-temperature decline under the modeled conditions, and how the relative importance of operating parameters differs between these two responses. To address this question, this study compares five well spacings and 14 multi-well configurations and separately evaluates three operating parameters using a three-factor, three-level orthogonal design.

Recent THM modeling studies provide a framework for examining the interactions among fluid flow, heat transport and reservoir deformation. However, recommendations for geothermal well layouts depend on the geological representation, completion conditions and operating assumptions adopted in each study. Their applicability to the Linqing sandstone reservoir therefore requires a site-specific assessment. In particular, hydraulic support and thermal interference need to be considered together: a configuration that limits groundwater drawdown may not necessarily maintain a higher production temperature. This motivates a comparative assessment of well spacing and geometry using both hydraulic and thermal indicators.

Accordingly, this study applies a three-dimensional THM model to the Linqing sandstone geothermal reservoir to compare five well spacings and 14 multi-well configurations. Groundwater drawdown and production temperature are evaluated as complementary performance indicators. A separate three-factor, three-level orthogonal analysis examines the effects of production rate, injection ratio and injection temperature. The contribution of this study is to characterize the configuration-dependent hydraulic–thermal trade-offs and distinguish the dominant operating parameters for the two responses under the modeled reservoir conditions.

2. Geological Background

2.1. Characteristics of Geological Structures

The study area is located in Linqing City, the northwest of Shandong Province (Figure 1), which is located in Linqing Depression of Mesozoic-Cenozoic fault basin. The regional structure was mainly influenced by the Yanshanian tectonic movement, and a series of NE-trending tensile faults developed. The main thermal control faults in the study area are Linqing fault, Guanxian fault and Tangyi fault, and the structural distribution presents a typical feature of “alternating ups and downs”. The above faults control the pattern of secondary uplift and depression in the area, such as Guantao uplift, Tangyi uplift, Linqing sag and Shenxian sag, etc. These structural units are regularly distributed alternately, forming a significant structural differentiation pattern. These geological structures play an important role in regulating the distribution and enrichment of geothermal resources and the characteristics of geothermal field.

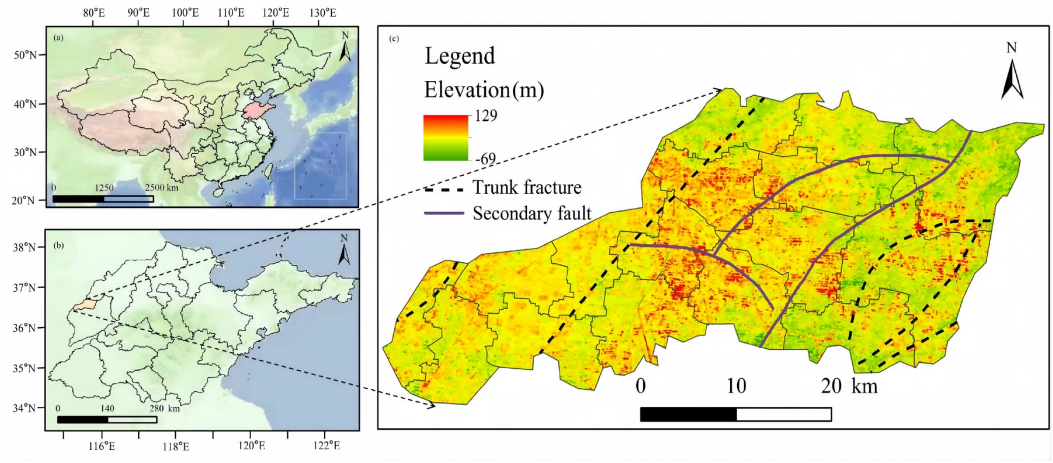


Figure 1. Overview map of study area.

2.2. Stratigraphic Distribution Characteristics

The geological evolution of the study area experienced multi-stage tectonic movements from Paleozoic to Cenozoic. The surface is covered by thick Quaternary loose sediments, and the basement and deep strata are developed from bottom to top: Neoarchean, Paleozoic, Mesozoic and Cenozoic. Cenozoic strata are the key to the occurrence of geothermal resources, which mainly include Paleogene, Neogene Guantao Formation, Neogene Minghuazhen Formation and Quaternary Plain Formation from bottom to top. The geothermal reservoir system in the study area is covered by the Quaternary and Neogene Minghuazhen Formation, in which the Neogene Guantao Formation sandstone reservoir is the main development target. The buried depth of the roof, the buried depth of the floor and the total thickness of the stratum are generally 1000~1200 m, 1350~1735 m and 370~580 m, respectively, and the buried depth of the floor is gradually deepening from southeast to northwest.

The aquifer of Guantao Formation thermal storage is mainly developed in the middle and lower part, and the lithology is mainly sandstone, gravel sandstone and glutenite. The accumulated thickness of thermal storage sandstone is generally 170~250 m, accounting for 37~45% of the total thickness of the stratum. The average thickness of single layer is 10~20 m, and the maximum single layer thickness is nearly 80 m. The reservoir is mainly heated by land heat flow, supplemented by deep circulation convection. The buried depth of the main production interval is between 1300~1700 m, and the wellhead water temperature is 58~67 °C, which belongs to warm water-hot water type low-temperature geothermal resources. From the geothermal profile, the geothermal gradient of Guantao Formation is 2.0~3.2 °C/100 m. The hydrochemical type of geothermal fluid in Guantao Formation is Cl-Na type, in which Na^+ and Ca^{2+} are the main cations and Cl^- and SO_4^{2-} are the main anions.

2.3. The Basic Theory of THM Coupling

The thermo-hydro-mechanical (THM) coupled numerical model developed is based on several fundamental assumptions. The soil is considered a fully saturated, isotropic and porous elastic medium, while the geothermal water within the reservoir is treated as an incompressible fluid. Fluid flow through the porous medium is assumed to obey Darcy's law, with heat conduction governed by Fourier's law and convective heat transfer described by Newton's law of cooling. Furthermore, the stress–strain behavior of the soil is characterized by linear thermoelastic theory, accounting for the effects of temperature

variations on mechanical deformation. These assumptions provide the theoretical basis for establishing the governing equations of the coupled THM model.

The mechanical field is solved via the quasi-static momentum balance with a thermo-poroelastic constitutive law. Temperature and stress changes affect the hydraulic field through porosity/permeability coupling. Because the present study focuses on the hydraulic and thermal performance of well configurations, the stress/strain fields are treated as intermediate coupling variables and are not presented in the main text.

2.3.1. Seepage Control Equation

During the production and injection process of geothermal water from hot reservoirs, since the pores within the soil are relatively small and uneven in distribution, the flow rate of geothermal water is slow. Therefore, its movement through the soil can be considered laminar flow. The seepage of geothermal water in soil obeys Darcy's law and satisfies the law of conservation of mass. For Darcy's law, under the influence of gravity, the seepage velocity of geothermal water can be expressed as [31]:

$$v = \frac{-k}{\mu}(\nabla p + \rho_w g \nabla z) \tag{1}$$

where v is the seepage velocity of geothermal water, m/s; k is the permeability of soil, m^2; μ is the dynamic viscosity of geothermal water, Pa · s; p is pore water pressure, Pa; g is the acceleration of gravity, generally take 9.8 m/s^2; ρ_w is the density of geothermal water, kg/m^3; z is the vertical coordinate in the coordinate system, which is positive in the direction.

According to the law of conservation of mass, the governing equation of geothermal water seepage in porous media can be expressed as:

$$\frac{\partial}{\partial t}(\varphi \rho_w) + \nabla \cdot (\rho_w v) = Q_m \tag{2}$$

$$S_p \frac{\partial p}{\partial t} + \nabla \cdot v + \alpha_B \frac{\partial \varepsilon_v}{\partial t} = Q_v \tag{3}$$

$$S_p = \frac{\varphi}{K_f} + \frac{\alpha_B - \varphi}{K_s} \tag{4}$$

$$\alpha_B = 1 - \frac{K_d}{K_s} \tag{5}$$

where ϕ is Porosity of porous media, t is time, s; Q_m is the quality source of geothermal water, $kg/(m^3 \cdot s)$; α_B is Biot's consolidation coefficient, ε_{vol} is volumetric strain; S is storage coefficient of geothermal resources storage layer, 1/Pa; K_f is volumetric modulus of geothermal water, 1/Pa; K_d is volumetric modulus of geothermal resources storage layer.

Substituting Darcy's law into the fluid mass balance equation yields the governing equation for groundwater flow:

$$S\frac{\partial P}{\partial \mathrm{t}} - \nabla \cdot \left(\frac{\mathrm{k}}{\mu_w}(\nabla p + \rho_w g \nabla z) \right) + \alpha_B \frac{\partial \varepsilon_v}{\partial t} = Q_v \tag{6}$$

2.3.2. Stress-Strain Control Equation

Under the quasi-static assumption, the mechanical response of the reservoir satisfies the equilibrium equation:

$$\nabla \cdot \sigma + \mathrm{f}_b = 0 \tag{7}$$

where σ is the total stress tensor, Pa; f_b is the body force per unit volume, N/m^3.

The mechanical response of the saturated porous reservoir is described using effective stress theory. Pore pressure contributes to the total stress and thereby influences the deformation of the reservoir skeleton. The relationship among total stress, effective stress and pore pressure is expressed as follows:

$$\sigma_{ij} = \sigma'_{ij} - \alpha_B \delta_{ij} p \tag{8}$$

$$\alpha = 1 - \frac{K_d}{K_s} \tag{9}$$

where σ_{ij} is total stress of soil; σ'_{ij} is effective stress of soil; p is pore water pressure, Pa; δ_{ij} is Kronecker symbol; α is experimental constant, usually α is close to 1; C_S is volume compression coefficient of soil particles; C is volume compression coefficient of porous media.

Under the assumption of small deformation, the reservoir skeleton is treated as an isotropic linear elastic medium. Its mechanical response is described by the stress–strain relationship incorporating the pore-pressure contribution [32]. The shear modulus is related to Young's modulus and Poisson's ratio as follows:

$$\varepsilon_{ij} = \frac{1+v}{E}\sigma_{ij} - \frac{v}{E}\sigma_{kk}\delta_{ij} + \frac{\alpha_B(1-2v)}{E}p\delta_{ij} \tag{10}$$

$$G = \frac{E}{2(1+v)} \tag{11}$$

where G is shear modulus; E is elastic modulus, MPa; ν is Poisson 's ratio; σ_{kk} is trace of the total stress tensor, Pa; ε_{ij} is components of the small-strain tensor; δ_{ij} is Kronecker delta.

Temperature changes produce thermal expansion or contraction of the reservoir skeleton. The resulting thermal strain is incorporated into the mechanical constitutive relationship through the temperature change, ΔT, relative to the reference thermal state:

$$\varepsilon_{ij} = \frac{1+v}{E}\sigma_{ij} - \frac{v}{E}\sigma_{kk}\delta_{ij} + \frac{\alpha_B(1-2v)}{E}\delta_{ij}p + \alpha_T\delta_{ij}\Delta T \tag{12}$$

where α_T is linear thermal expansion coefficient, K^{-1}; ΔT is temperature change relative to reference state, K.

Combining the elastic response with the pore-pressure and thermal contributions gives the coupled constitutive relationship below:

$$\sigma_{ij} = 2G\varepsilon_{ij} + \lambda_L\varepsilon_v\delta_{ij} - \alpha_B\delta_{ij}p - 3K_d\delta_{ij}\alpha_T\Delta T \tag{13}$$

where λ_1 is Lame constants, ε_v is volumetric strain.

2.3.3. Heat Transfer Control Equation

In porous thermal storage, heat transfer mainly depends on heat conduction and thermal convection. The governing equation of heat transfer in thermal reservoir can be expressed as [33]:

$$\left(\rho C_p\right)_{eff}\frac{\partial T}{\partial t} + \rho_w C_{p,w}\mathrm{v}\cdot\nabla T - \nabla\cdot(\lambda_{eff}\nabla T) = Q_T \tag{14}$$

where Q_T is heat source, W/m; λ is thermal conductivity, W/(m·°C); C_w is specific heat capacity of geothermal water, J/(kg·°C); T is temperature of the geothermal system, °C. ρ_w is the density of geothermal water, kg/m^3; v is the seepage velocity, m/s; $\left(\rho C_p\right)_{eff}$ is the effective volumetric heat capacity of the saturated porous medium (J/(m^3·K)); λ_{eff} is the effective thermal conductivity of the saturated porous medium (W/(m·K)).

The effective volumetric heat capacity and thermal conductivity of the saturated porous medium are expressed as follows:

$$\left(\rho C_p\right)_{eff} = (1-\varphi)\rho_s C_{p,s} + \varphi\rho_w C_{p,w} \tag{15}$$

$$\lambda_{eff} = (1-\varphi)\lambda_s + \varphi\lambda_w \quad (16)$$

where ρ_s and ρ_w are the densities of the rock matrix and geothermal water, respectively (kg/m^3); $C_{p,s}$ and $C_{p,w}$ are their specific heat capacities (J/(kg·K)); and λ_s and λ_w are their thermal conductivities (W/(m·K)).

Substituting Equations (15) and (16) into Equation (14), the governing heat transfer equation can be rewritten as:

$$\left[(1-\varphi)\rho_s C_{p,s} + \varphi\rho_w C_{p,w}\right]\frac{\partial T}{\partial t} + \rho_w C_{p,w} v \cdot \nabla T - \nabla \cdot [((1-\varphi)\lambda_s + \varphi\lambda_w)\nabla T] = Q_T \quad (17)$$

where the symbols ρ and C denote the density and specific heat capacity of the medium, respectively.

2.3.4. Solving Conditions of THM Coupling Model

The solution of THM coupled numerical model needs to set initial conditions and boundary conditions. For boundary conditions, it can be divided into three categories: The Dirichlet boundary conditions are the known water head, temperature and displacement of the study area on the boundary; The Neumann boundary condition involves knowing the flow rates and heat flux densities at points on the plane perpendicular to the boundary within the study area. The Cauchy boundary condition involves knowing the heat exchange conditions along the boundary of the study area.

The initial conditions of the model refer to the states of the deformation field, seepage field and temperature field in the study area at the initial moment, with respect to the corresponding variables. The initial condition for the deformation field is the amount of deformation at that time, the initial condition for the seepage field is the water pressure at that moment, and the initial condition for the temperature field is the temperature value at that time.

3. THM Coupling Model

3.1. Model Geometry and Parameters

A multi-field coupled numerical model of THM in geothermal reservoir production is established based on the actual strata in the main urban area of Linqing City, Shandong Province, that is, the strata obtained from geothermal wells lq5~lq57. The numerical model divides the strata into four layers (Figure 2). From the surface downwards, they are: Quaternary (Q), Minghuazhen Formation (N_2m), Guantao Formation (N_1g) and Dongying Formation (E_3d).

The main lithology of the Quaternary is silty clay, silty sand, fine sand, clayey silty sand and clay, with a layer thickness of 270 m. The main lithology of the Minghuazhen Formation is mudstone, silty sand, fine sand and gray-green gravel sandstone with a thickness of 833 m. The Guantao Formation is mainly composed of mudstone, siltstone and gravelly sandstone, which is the main thermal storage aquifer in this area with a thickness of 611 m. Dongying Formation is dominated by mudstone with a small amount of siltstone, medium-fine sandstone and sandy mudstone, with a thickness of 286 m.

Each geological layer was represented as a homogeneous unit, retaining the property contrasts between formations but not explicitly resolving the sandstone, gravelly sandstone and mudstone interbeds within the Guantao Formation. This simplification allows the effects of well spacing and configuration to be compared under a consistent geological representation. However, local permeability contrasts may redistribute flow within the reservoir: connected high-permeability intervals may enhance hydraulic communication and cold-water migration between wells, whereas low-permeability interbeds may restrict

interlayer exchange. The homogeneous representation may therefore smooth local hydraulic and thermal responses and influence the predicted differences among well configurations.

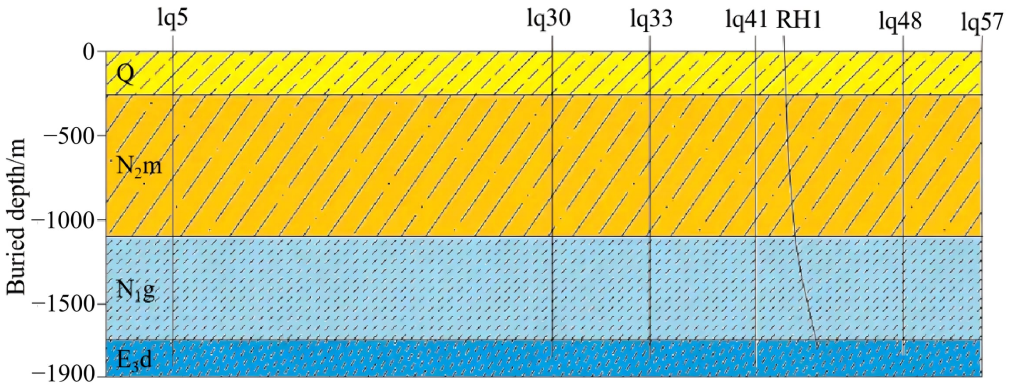


Figure 2. Geological profile of the study area.

The computational domain extended 10,000 m in both horizontal directions and 1550 m in depth. The model top was located at z = 0, with the vertical coordinate decreasing downward. The model geometry is shown in Figure 3a.

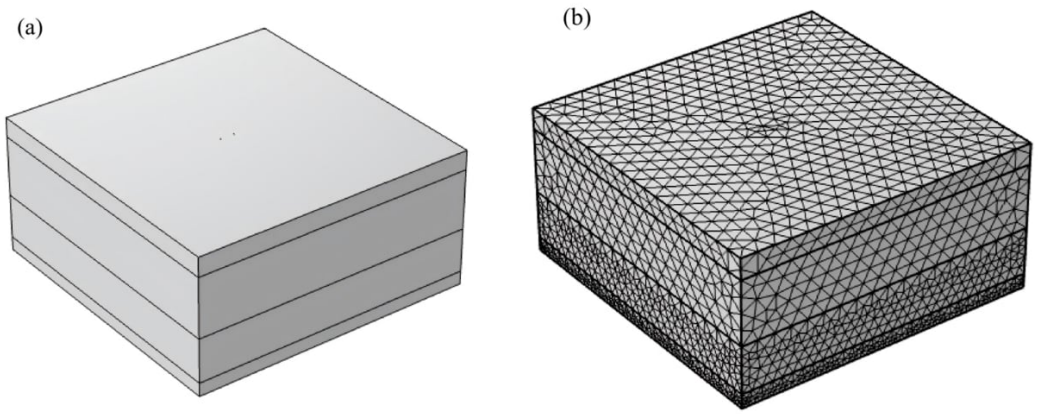


Figure 3. Fluid-solid-thermal coupling numerical model: (**a**) geometric model; (**b**) mesh generation.

The computational domain was discretized using free tetrahedral elements, as shown in Figure 3b. The mesh sequence included finer and extra-fine size settings to provide different spatial resolutions within the domain.

The production and injection wells were represented as vertical line segments extending to a depth of 1550 m. For the doublet configurations, well spacing was defined as the horizontal straight-line distance between the production and injection well axes. The multi-well arrangements are illustrated in the corresponding configuration figures. All scenarios used identical well depths and active production–injection intervals, with only the horizontal well positions being changed.

The soil parameters of each stratum taken in this study are based on the relevant engineering geological investigation report, geotechnical test results in northwest Shandong Province. The range of physical and mechanical parameters of the numerical model is shown in Table 1.

Table 1. Physical and mechanical parameters of rock soil.

Stratum	Elastic Modulus (MPa)	Density (kg/m^3)	Poisson's Ratio	Porosity	Permeability (m^2)	Thermal Conductivity (W/(m·K))	Heat Capacity at Constant Pressure (J/(kg·K))	Thermal Expansion Coefficient (1/K)
Q	80	1.97~2.02	0.22~0.25	0.28~0.37	4.79×10^{-15}~ 1.61×10^{-14}	1.03~1.35	820~870	1.0×10^{-5}
N_2m	180	1.99~2.20	0.31~0.40	0.11~0.24	6.3×10^{-14}~ 7.2×10^{-14}	1.48~1.77	820~900	1.3×10^{-5}
N_1g	350	1.88~2.18	0.30~0.35	0.15~0.35	2.3×10^{-14}~ 4.53×10^{-13}	1.74~1.91	850–948	8.5×10^{-6}
E_3d	370	2.03~2.22	0.30~0.33	0.13~0.31	1.4×10^{-14}~ 3.80×10^{-13}	1.80~1.91	850–950	7.1×10^{-6}

The dynamic viscosity and density of geothermal water were treated as constants, with values of 1.01×10^{-3} Pa·s and 1000 kg/m^3, respectively. Their temperature dependence was not included in the present simulations. This simplification excludes the effects of temperature-induced changes in these fluid properties on the predicted hydraulic and thermal responses and constitutes a limitation of the model.

3.2. Initial Conditions and Boundary Conditions

The model boundary conditions are classified into mechanical, hydraulic and thermal conditions. Fixed constraints are applied to the bottom of the model, with zero normal displacement imposed on all lateral boundaries. Both the upper and lower surfaces are treated as impermeable and adiabat ic boundaries, with no water or heat exchange across these surfaces. The lateral boundaries are prescribed as constant-head boundaries, where the hydraulic head remains unchanged throughout the simulation. The constant flow rates for both the injection and production wells are set at 1500 m^3/day, with an injection-to-production ratio of 1:1. The constant-head boundaries represent an idealized surrounding groundwater system in which the hydraulic head at the model margins is maintained during production and injection.

The initial temperature field is defined by a linear geothermal gradient of 0.023 °C/m, with a temperature of 26 °C at the model top. The initial temperature therefore increases linearly with depth below the model top. The injection temperature is set at 20 °C, and heat exchange is permitted across the lateral boundaries. The fixed bottom represents an idealized mechanically constrained base. The lateral constraints prevent displacement normal to the model sides while permitting tangential movement, approximating the confinement imposed by the surrounding geological medium. This treatment excludes external heat supply through the upper and lower boundaries, allowing the simulations to examine heat redistribution within the modeled domain under production–injection conditions. It is an idealization and does not explicitly represent regional conductive heat replenishment.

3.3. Numerical Solution Procedure

The model was implemented using the finite element method in COMSOL 5.6 Multiphysics. The solution sequence comprised a stationary study and a time-dependent study, with the latter configured to use an existing solution for initialization. Time integration employed an implicit backward differentiation formula (BDF) with orders ranging from one to two and adaptive internal time stepping. A fully coupled nonlinear solver was enabled for the time-dependent study, and PARDISO was configured as a direct linear solver. The production–injection responses were evaluated over a 30-year period.

The numerical model is verified through mesh-independence tests and time-step convergence tests, and its parameters are constrained by available site data. However, a direct comparison with long-term field measurements or published analytical solutions is not included in this study. The model is therefore used for the relative comparison of well configurations and operating parameters rather than for site-specific long-term prediction.

3.4. Model Calibration and Validation

To evaluate the reliability of the geothermal water flow model, the simulated geothermal water levels were compared with field monitoring data. As illustrated in Figure 4a, the simulated water levels reproduce the overall temporal variations observed during the monitoring period. The change in geothermal water level within the time series is 19.91 m, and the maximum error between the monitored geothermal water level and the simulated value is 1.58 m, which is less than the maximum allowable error (2 m). These comparisons indicate that the geothermal water flow model can reasonably reproduce the observed hydraulic response under the investigated operating conditions, providing support for the subsequent analysis of geothermal production and reinjection processes.

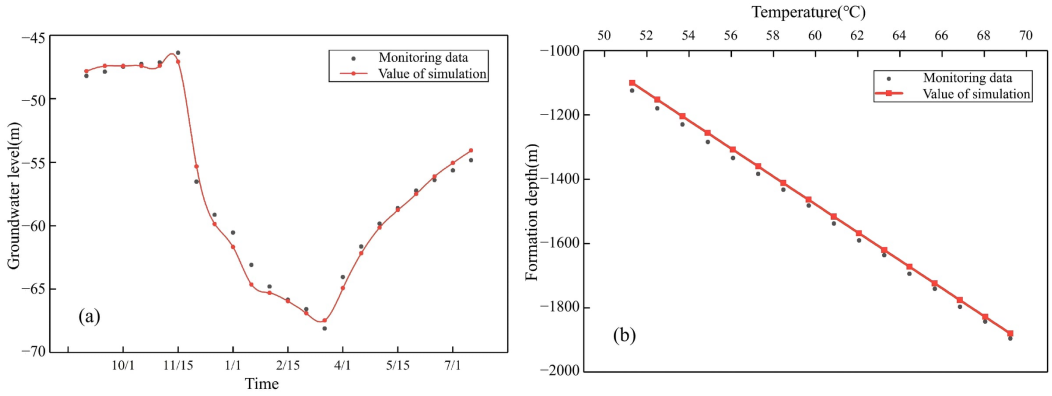


Figure 4. Model accuracy verification: (**a**) geothermal water level; (**b**) temperature.

The thermal model was evaluated by comparing the simulated temperature distributions with production well temperatures. The initial temperature field was established using an upper boundary temperature of 25 °C and a geothermal gradient of 0.023 °C/m. The simulated temperature profile was first compared with temperature measurements from the geothermal well. As shown in Figure 4b, the simulated temperature distribution is generally consistent with the observed vertical temperature profile. The maximum error between the monitoring results and simulation results of extraction temperature is 0.6 °C, and the average error is 0. 26 °C, indicating that the model can reasonably represent the geothermal gradient and initial thermal conditions of the reservoir.

4. Results Analysis

4.1. Reasonable Well Pattern

4.1.1. Geothermal Double Well System

Geothermal energy has been widely used in wells in the suitable area of geothermal reservoir production, but there is no uniform standard for the spacing between wells and the influence of well spacing on the flow field and temperature field of thermal storage has not been well revealed. When the distance between wells is too large, it will often lead to the increased groundwater drawdown in thermal reservoirs; if the spacing between wells is too small, the production temperature of geothermal wells will drop rapidly, so it is necessary to study the reasonable spacing between geothermal wells. Since the distance between wells

in the study area is between 100 m and 1000 m, this study has set five different distance gradients of 200 m, 400 m, 600 m, 800 m and 1000 m, and the simulation time is 30 years. According to the changes of groundwater level and production temperature under different spacing between wells, the reasonable spacing between wells is determined.

Figure 5 shows that with the gradual increase of the distance to the well, the water level at the center of the groundwater depression cone is getting bigger and bigger, and the water level at the injection well is also getting bigger and bigger. The groundwater drawdown is 0.36 m when the distance between wells is 200 m and the continuous production and injection is 30 years, and the rise and fall of groundwater level at production wells and injection wells are roughly symmetrical.

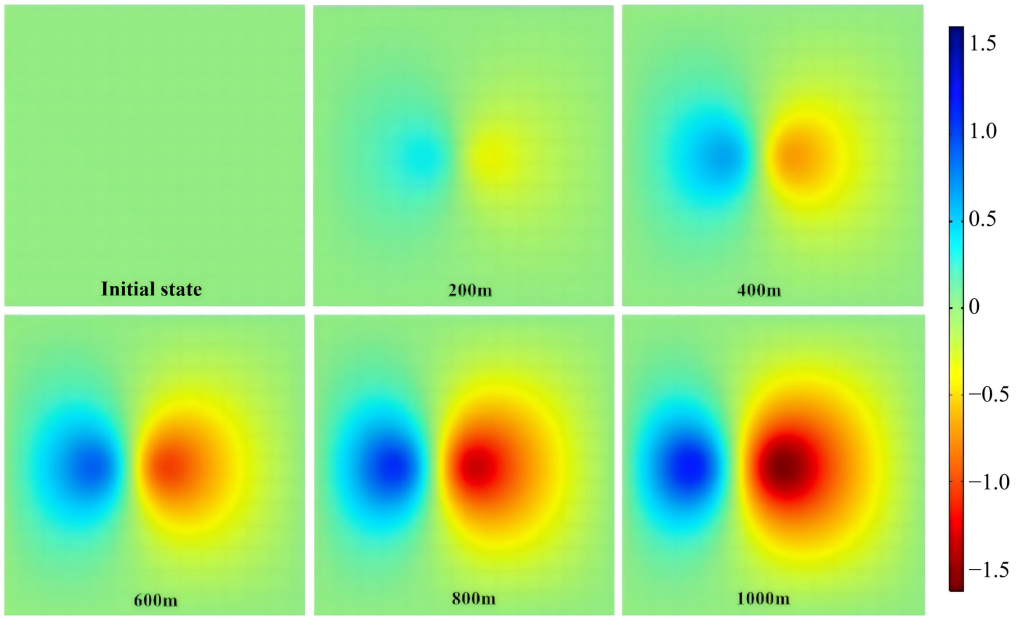


Figure 5. Geothermal water level for 30 years under different well spacing (m).

As the distance between the wells increases, the variation in water levels between the production well and the injection well becomes less symmetric. Specifically, the downward trend of the water level in the production well becomes more pronounced than the upward trend in the injection well, and the gap between the two continues to widen over time. When the distance between wells is 1000 m and the continuous production and injection is 30 years, the groundwater drawdown reaches 1.62 m, which is about 4.5 times of that when the distance between wells is 200 m.

As shown in Figure 6, with the increase in the distance from the well, the temperature change at the injection well is almost the same, and the temperature drops to about 20 °C, but the geothermal water temperature at the production well is less affected.

Figure 7 shows the specific changes of groundwater level and production temperature with time. Figure 7a shows that with the increasing distance between geothermal water and the well, groundwater drawdown is also increasing, and the time for the groundwater level to stabilize is also getting longer. When the distance between wells is 200 m, the groundwater drawdown is 0.16 m, and it tends to be stable for 1 year. However, when the distance between wells is 1000 m, the groundwater drawdown is about 1.56 m, which takes about 2.5 years to stabilize, and the groundwater drawdown is about 9.8 times as much as when the distance between wells is 200 m. Therefore, if only the change in groundwater level caused by thermal storage production is considered, it is obvious that the smaller the well spacing is, the best situation is 200 m.

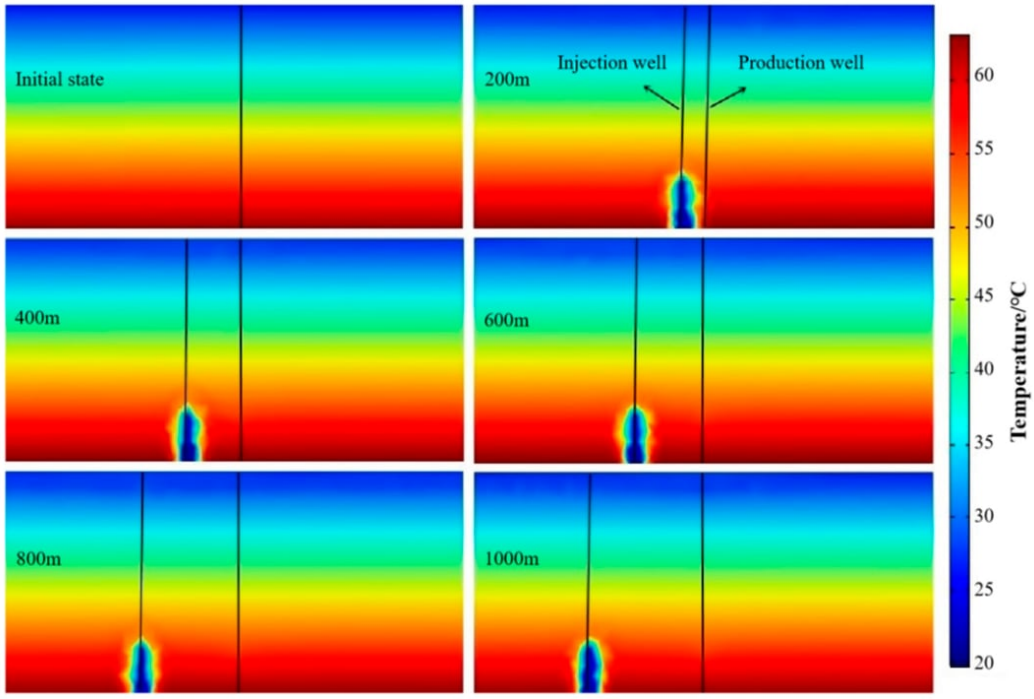


Figure 6. The temperature of the model running for 30 years under different well spacing (°C).

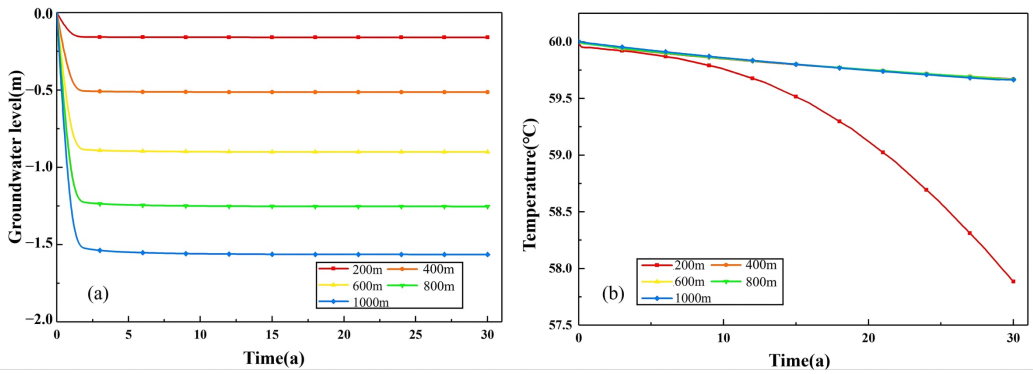


Figure 7. The change of groundwater level and production temperature under different well spacings: (**a**) water level; (**b**) temperature.

As shown in Figure 7b, when the spacing between wells is 200 m, the production temperature will decrease by about 2.12 °C after 30 years of production and injection, and with the extension of production and injection time, the downward trend of the production temperature will become faster and faster from the initial slow decline. The variation range of production temperature is almost the same in other cases, and the rate of temperature decrease has not changed greatly. After 30 years of production and injection, the production temperature decreases by about 0.34 °C. The best case is when the distance between wells is 400 m, if only the production temperature change caused by geothermal production is considered. Therefore, considering the changes in groundwater level and production temperature, the optimal spacing between wells is 400 m.

4.1.2. Reasonable Arrangement Scheme of Geothermal Multi-Wells

In the arrangement of geothermal wells in the suitable area of geothermal reservoir production, there is not only the situation of aligning wells. The comparative advantages of single well and multi-well schemes still need further study. To further demonstrate

the rationality of the multi-well layout schemes, this paper proposes three layout options: "two injection and one production" well pattern, "one injection and two production" well pattern, and "two injection and two production" well pattern. For the "two injection and one production" well pattern and the "one injection and two production" well pattern, five configurations are set up. For the "two injection and two production" well pattern, four configurations are set up. The specific layout is shown in Figure 8. As mentioned above, the spacing between any two wells is 400 m.

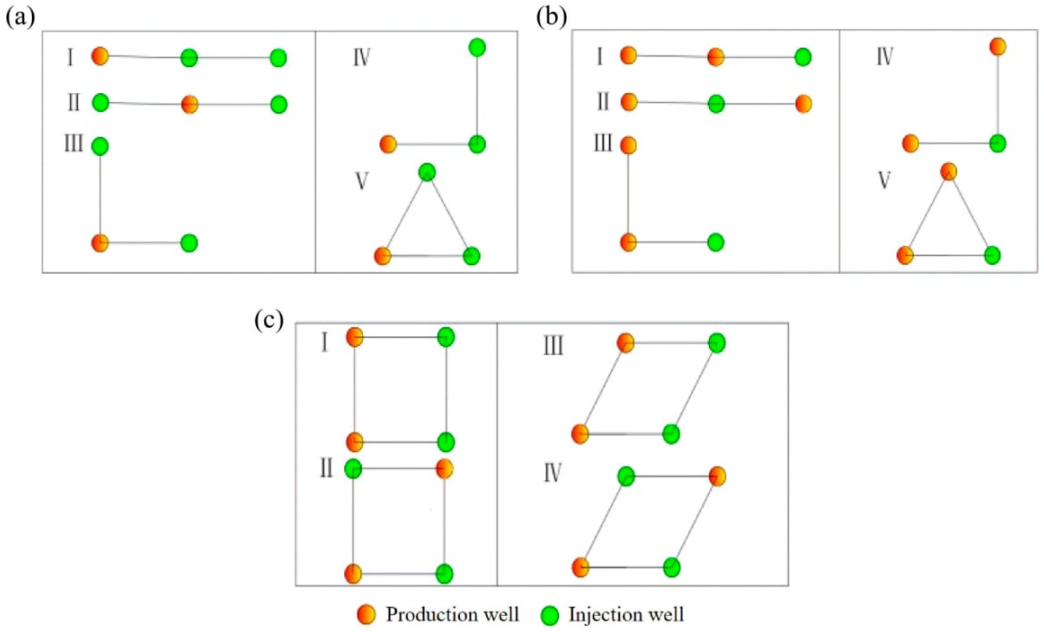


Figure 8. Geothermal multi-well layout pattern: (**a**) "two injection and one production" well pattern (**b**); "one injection and two production" well pattern; (**c**) "two injection and two production" well pattern.

(1) "Two injection and one production" well pattern

For the well pattern of "two injection and one production", the constant production of the production wells is set to 1500 m^3/d, the injection quantity of each of the two injection wells is 750 m^3/d, and the injection time is 30 years. The production well is always located in the center of the numerical pattern, and the change result of groundwater level calculated by the numerical model is shown in Figure 9.

The change in groundwater level on the surface of thermal reservoir is shown in Figure 9. It can be seen that among the five well patterns of "two injection and one production", the second groundwater level has the smallest decline, only −0.51 m, the variation range of the groundwater level is roughly elliptical, and the water level rise on both sides of the production well is roughly symmetrical. The second is well Patterns III and V, and the decrease in groundwater level is 0.65 m and 0.69 m, respectively. Although there is little difference between them, the upward trend of water level in Pattern V is greater than that in Pattern III. Pattern I has the largest decrease in groundwater level, which is 1.03 m, about twice as much as in Pattern II. Therefore, if we only consider the decrease in groundwater level, well Pattern II is obviously better.

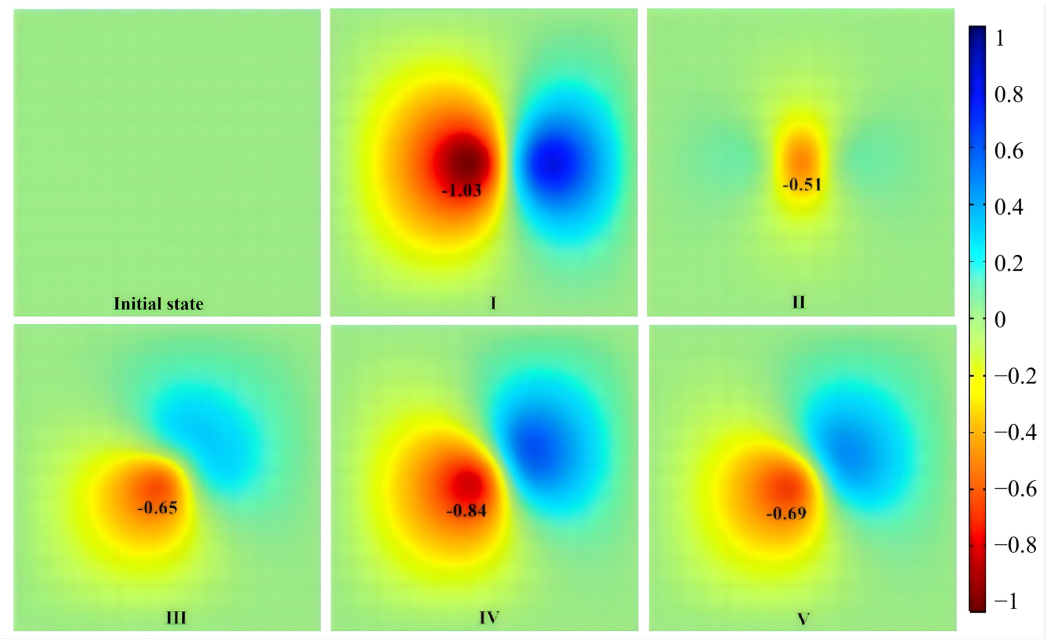


Figure 9. Groundwater level under five well patterns (m).

The change in groundwater level at the production well far away from the injection well is shown in Figure 10a. As can be seen from Figure 10a, the groundwater level in Patterns II, III, and V is almost the same, with a decrease of about 0.5 m, and the groundwater level can be stabilized within two years. Followed by Pattern IV, the groundwater drops by 0.65 m. The decrease in groundwater level in Pattern I is the largest, about 0.88 m, which is 0.38 m more than that in Patterns II, III, and V, and it takes the longest time for groundwater level to stabilize, about 7 years. As far as the decrease in groundwater level is concerned, Pattern II is the best among the five patterns.

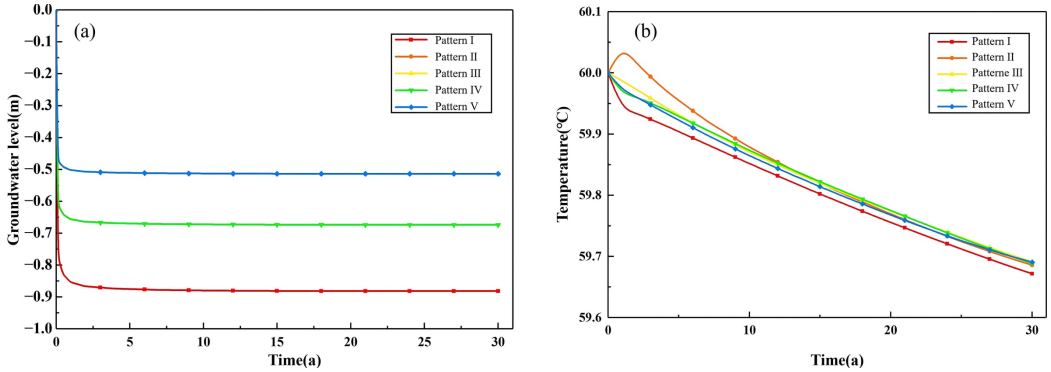


Figure 10. Groundwater level and production temperature change under five well patterns: (**a**) water level; (**b**) production temperature.

The variation in production temperature of the production well close to the injection well is shown in Figure 10b. It can be seen from Figure 10b that the production temperature of Pattern II decreases the slowest, followed by Pattern III, Pattern IV and Pattern V, and Pattern I decreases the fastest, and the production temperature of Pattern I is always in the lowest state. The production temperature decline of five models in 30 years is 0.33 °C, and the temperature difference of different well patterns is relatively small. This just shows that the well spacing of 400 m is enough for production temperature, and no matter how the well pattern changes, it has little influence on the production temperature. Therefore,

considering the changes in groundwater level and production temperature, well Pattern II is the best in the "two injection and one production" well pattern.

(2) "One injection and two production" well pattern

For the well pattern of "one injection and two production", the constant injection amount of injection wells is 1500 m^3/d in the numerical model, the production amount of each of the two production wells is 750 m^3/d, and the production and injection time is 30 years. The production well is always located in the center of the numerical model, and the change result of groundwater level calculated by the numerical model is shown in Figure 11.

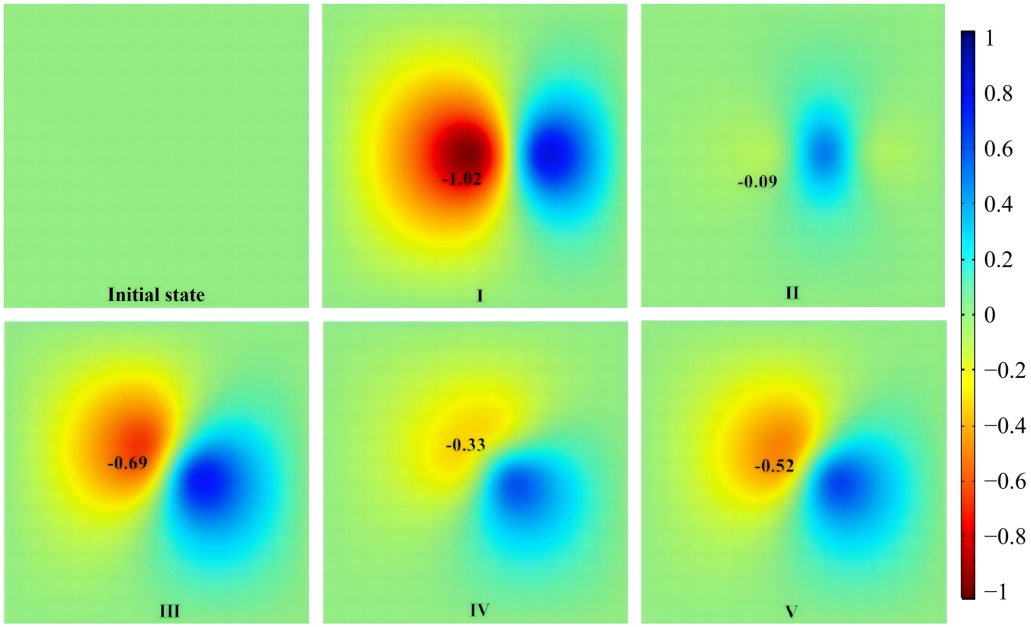


Figure 11. Groundwater level under five well patterns (m).

The change in groundwater level on the surface of the thermal reservoir is shown in Figure 11. From this figure, it can be seen that among the five well patterns of "one injection and two production", the decline in groundwater level in the second well pattern is the smallest, only 0.09 m, and the water level change at the injection well is roughly elliptical under the influence of the production wells on both sides.

Well Patterns IV and V are 0.33 m and 0.52 m, respectively, in which the decrease and increase in groundwater level in Pattern IV are greater than that in Pattern IV. In Pattern I, the groundwater level drops the most, which is 1.02 m, which is about 11.3 times that in Pattern II. Therefore, if we only consider the decrease in groundwater level, the effect of well Pattern II is better.

The change in groundwater level on the surface of the thermal reservoir at the production well far away from the injection well is shown in Figure 12a. The groundwater level at the production well rises in Pattern II, which is about 0.1. In other patterns, the groundwater level is in a state of decline, and the groundwater level at the production well in Pattern IV has a small decline, about −0.1 m. In Pattern I, the decrease in groundwater level at the production well is the largest, about 1 m. Combined with Figure 12, in terms of groundwater level decline, Pattern II is the best among the five patterns.

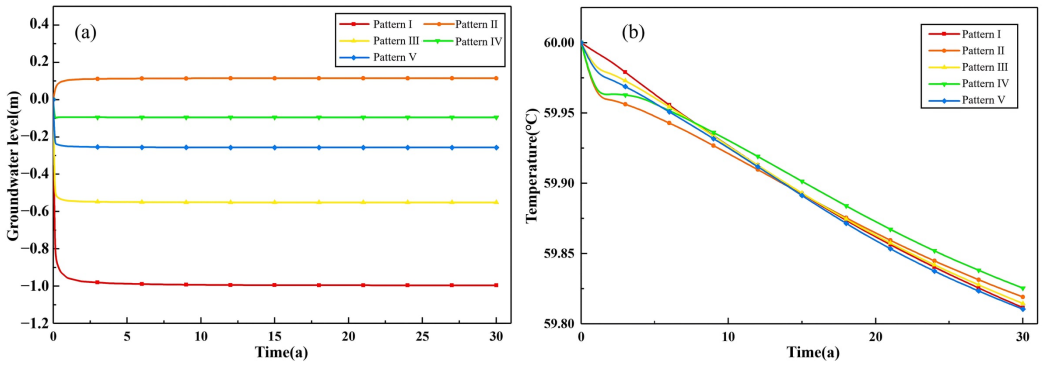


Figure 12. Groundwater level and production temperature change under five well patterns: (**a**) water level; (**b**) production temperature.

The variation in production temperature of the production well near the injection well is shown in Figure 12b. During the period of production and injection, the production temperature difference of the five well patterns is less than 0.1 °C. During 30 years of production, the production temperature in Pattern IV is the highest, followed by Pattern II, and the production temperature in Pattern V is the lowest, but the temperature difference in several patterns is small. Therefore, in the "one injection and two production" well pattern, Pattern II is the best.

(3) "Two injection and two production" well pattern

For the well pattern of "two injection and two production", the injection quantity of each of the two injection wells is 750 m^3/d, the production quantity of each of the two production wells is 750 m^3/d, and the injection time is 30 years. One of the production wells is always located in the center of the numerical model, and the change result of groundwater level calculated is shown in Figure 13. From this figure, it can be seen that in the four well patterns of "two injection and two production", the decrease in groundwater level in the fourth stage is the smallest, only 0.11 m, and the decrease in groundwater level is roughly symmetrical along the arc region where groundwater level rises.

Well Pattern II is 0.15 m, and the declining area of the groundwater level is roughly symmetrical with the rising area of the groundwater level. The other two models have a large drop in groundwater level, both of which are greater than 0.65 m, which is about 5.9 times that of well Pattern IV, and there are obvious water level drop funnels at the drop in groundwater level. Therefore, if we only consider the decrease in groundwater level, the effect of well Pattern IV is better.

The change in groundwater level on the surface of the thermal reservoir at the production well far away from the injection well is shown in Figure 14a. From Figure 14, it can be seen that in Pattern IV, the groundwater level at the production well rises, about 0.02 m. In other patterns, the groundwater level is in a state of decline, and the groundwater level at the production well in Pattern II has a small decline of about 0.1 m. In Pattern III, the decrease in groundwater level at the production well is the largest, about 0.53 m. As far as the decrease in groundwater level is concerned, Pattern IV is the best among the four patterns.

The production temperature change in one of the production wells is shown in Figure 14b. The production temperature changes of Patterns I and II are approximately the same, and the temperature changes in Patterns III and IV are approximately the same. Different from the latter, Patterns I and II will have a rapid temperature drop in the first year of production, a slight temperature rise in the next three years, and a relatively stable temperature drop stage after five years. During 30 years of production, the production temperature in Pattern IV is the highest, followed by Pattern II, and the temperature differ-

ence between them is less than 0.1 °C. Therefore, considering the changes in groundwater level and production temperature, Pattern IV is the best among the four well distribution patterns of "two injection and two production".

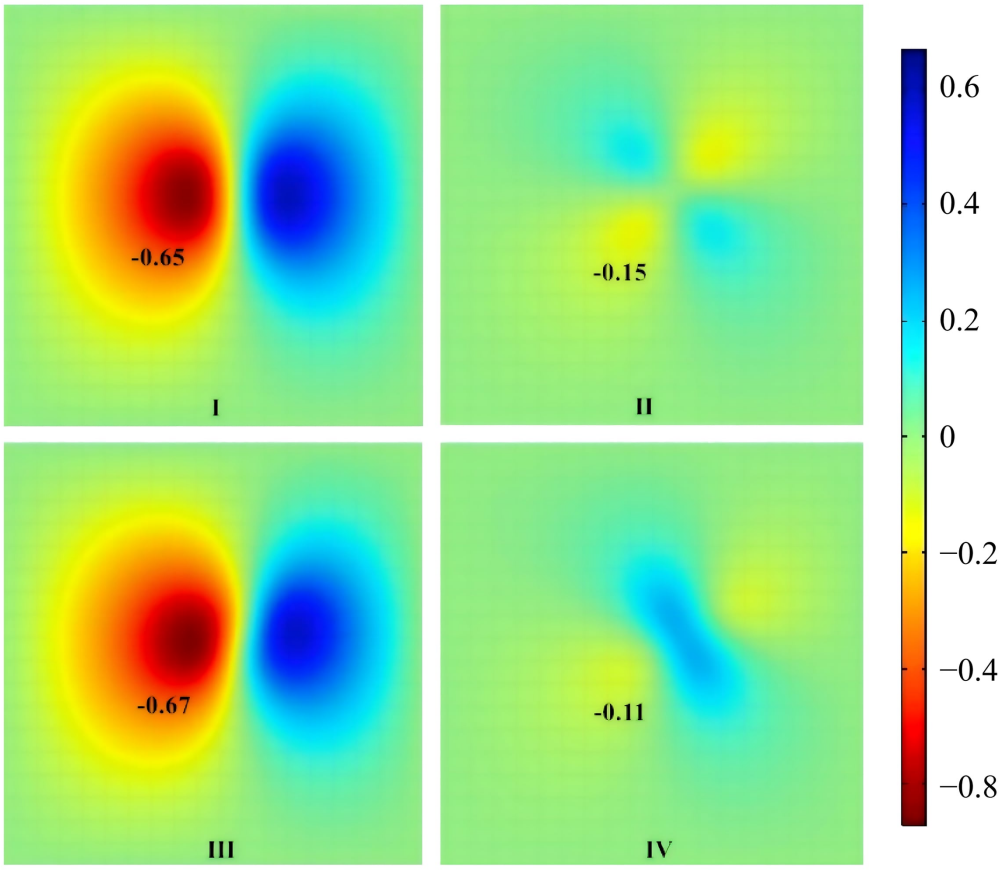


Figure 13. Groundwater level under four well patterns.

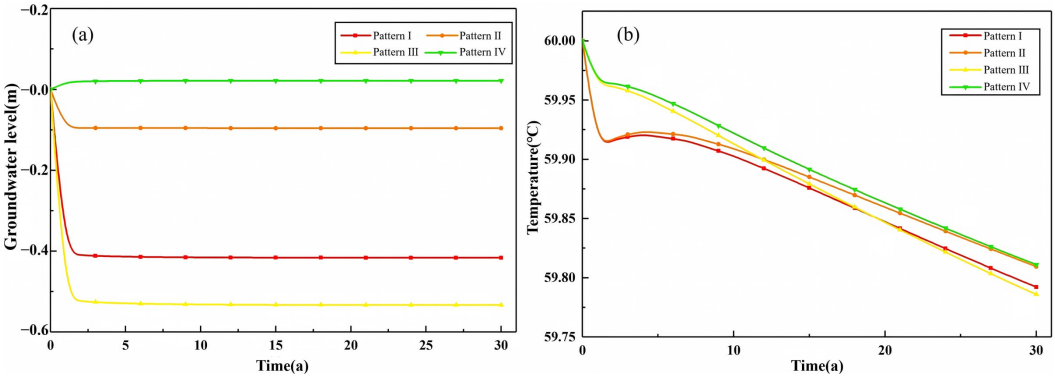


Figure 14. Groundwater level production temperature change under four different well patterns: (**a**) groundwater level; (**b**) production temperature.

To sum up, there are 14 well patterns in the above three layout schemes. For the well pattern of one production and two injection, Pattern II can be selected, that is, three wells are placed in a straight line and the production well is placed in the middle of two injection wells. For the well pattern of "two injection and two production", Pattern II can be selected, that is, three wells are placed in a straight line and the injection well is placed in the middle of two production wells. For the well pattern of two production and two injection, Pattern

IV can be selected, that is, four wells are arranged in a diamond shape and two injection wells are located diagonally.

4.2. Sensitivity Analysis of Production and Injection

4.2.1. Test Scheme Design

As far as the production and injection performance of thermal storage is concerned, the main influencing factors that can be artificially regulated are the production rate of geothermal water, the recharge rate of geothermal tail water and the recharge temperature of geothermal tail water. The injection rate, rather than the injection quantity, is used as one of the influencing factors here, mainly because if the injection quantity is used here, the injection quantity will be greater than the production quantity in the design process of the orthogonal test, which is not in line with the actual situation that geothermal tail water is used for injection.

In order to quantitatively analyze the influence degree of various influencing factors on the production temperature of geothermal reservoir geothermal water flow field, nine groups of orthogonal tests with three factors and three levels will be designed by the orthogonal test design method, and then the initial temperature of the numerical model is consistent with the previous section by calculating the numerical model with a well spacing of 200 m. The specific arrangement of the test is shown in Tables 2 and 3.

Table 2. Influencing factors and level design.

Level	Production (m^3/d)	Injection Rate (%)	Injection Temperature (°C)
1	1500	100	20
2	2250	80	30
3	3000	60	40

Table 3. Orthogonal test scheme design and calculation results.

Level	Production (m^3/d)	Injection Rate (%)	Injection Temperature (°C)	Groundwater Level Drop (m)	Production Temperature (°C)
1	1500	100	20	0.16	57.88
2	1500	80	40	0.66	59.06
3	1500	60	30	1.17	59.15
4	2250	100	40	0.25	57.43
5	2250	80	30	1.02	57.12
6	2250	60	20	1.80	57.34
7	3000	100	30	0.32	54.10
8	3000	80	20	1.33	54.25
9	3000	60	40	2.34	57.61

4.2.2. Analysis of Test Results

(1) Range analysis

Range refers to the difference between the maximum value and the minimum value between different levels of the same influencing factor. The range analysis includes two steps: calculation and judgment, which can measure the data dispersion, quantify the influence degree of each factor, identify the main and secondary factors and find the optimal combination [34].

Range analysis was performed by taking the groundwater level variation and production temperature obtained from the orthogonal experiment at each level as the indicator response values, so as to determine the degree of influence of each factor on its response value. The calculation results are shown in Table 4.

Table 4. Range analysis of index response value.

Parameter	Groundwater Drawdown (m)	Production Temperature (°C)
Production	0.67	3.38
Injection rate	1.53	1.56
Injection temperature	0.26	1.54

The range analysis process determines the sensitivity of different levels of a single factor to the indicator response values on the basis of excluding the other two influencing factors. As can be seen from Table 4, the influencing factors for groundwater drawdown, in descending order of influence, are geothermal tail water injection rate, geothermal water production volume and geothermal tail water injection temperature; the influencing factors for production temperature, in descending order of influence, are geothermal water production volume, geothermal tail water injection rate and geothermal tail water injection temperature. Figures 15 and 16 show the corresponding relationship between the mean values of different influencing factors at each level and the indicator response values.

As shown in Figure 15, the groundwater level drawdown gradually increases with increasing production volume, and the drawdown is roughly positively correlated with the geothermal water production volume. At production volumes of 1500 m^3/d, 2250 m^3/d and 3000 m^3/d, the groundwater level drawdowns were 0.66 m, 1.02 m and 1.33 m, respectively. The drawdown gradually decreases with increasing geothermal tail water injection rate, and the drawdown is roughly negatively correlated with the geothermal tail water injection rate.

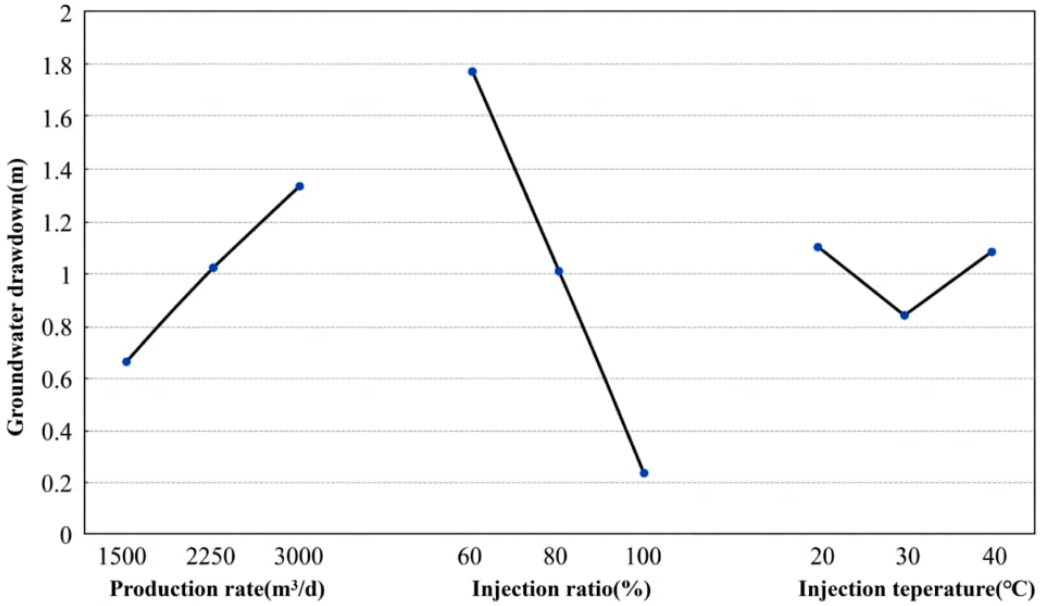


Figure 15. Groundwater level change at different levels of different influencing factors.

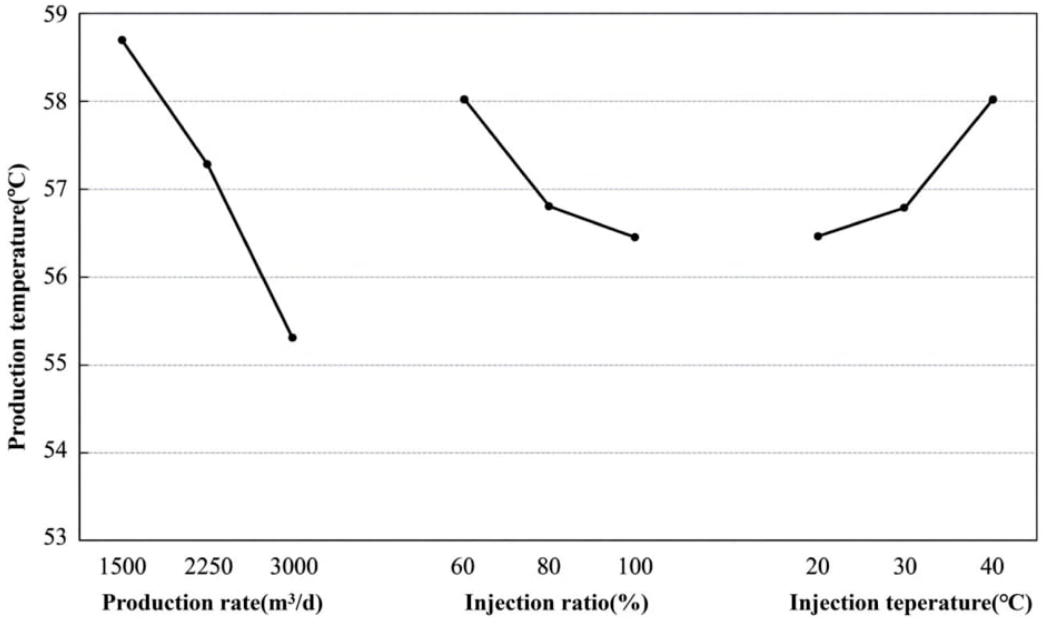


Figure 16. Exploiting temperature changes at different levels of different influencing factors.

At injection rates of 60%, 80% and 100%, the drawdowns were 1.77 m, 1.00 m and 0.24 m, respectively. There is no linear relationship between the groundwater level and the injection temperature as the injection temperature increases; therefore, the groundwater level drawdown is not greatly affected by the injection temperature and is mainly affected by the geothermal water production volume and the tailwater injection rate.

As shown in Figure 16, the production temperature gradually decreases with increasing production volume, and the production temperature is roughly negatively correlated with the geothermal water production volume. At production volumes of 1500 m^3/d, 2250 m^3/d and 3000 m^3/d, the production temperatures of geothermal water were 58.70 °C, 57.30 °C and 55.32 °C, respectively. The production temperature gradually decreases with increasing injection rate, and the decrease rate of the production temperature at a geothermal tail water injection rate of 60~80% is markedly faster than that at a tail water injection rate of 80~100%. At geothermal tail water injection rates of 60%, 80% and 100%, the production temperatures were 58.03 °C, 56.81 °C and 56.47 °C, respectively.

The production temperature gradually increases with increasing injection temperature, and the increase rate of the production temperature at an injection temperature of 30~40 °C is markedly faster than that at an injection temperature of 20~30 °C. At injection temperatures of 20 °C, 30 °C and 40 °C, the production temperatures were 56.49 °C, 56.79 °C and 58.03 °C, respectively. Therefore, the production temperature is simultaneously affected by the geothermal water production volume, tail water injection rate and injection temperature, and it is affected more strongly by the geothermal water production volume.

(2) Variance analysis.

Analysis of variance (ANOVA) was performed to quantify the main effects of the three operating parameters. The nine-run orthogonal design provided eight total degrees of freedom: two for each factor and two for the unassigned column. The unassigned-column sum of squares was divided by its degrees of freedom to obtain the error mean square. The F statistic for each factor was calculated as the ratio of its mean square to the error mean square, and the corresponding p value was determined using an F distribution with two numerator and two denominator degrees of freedom. The results are presented in Tables 5 and 6.

Table 5. Analysis of variance for groundwater drawdown.

Source	Sum of Squares	Degrees of Freedom	Mean Square	F	*p*
Production rate	0.6681	2	0.334	5.268	0.160
Injection ratio	3.4961	2	1.748	27.570	0.035
Injection temperature	0.1286	2	0.064	1.014	0.496
Error (unassigned column)	0.1268	2	0.0634	—	—

Table 6. Analysis of variance for production temperature.

Source	Sum of Squares	Degrees of Freedom	Mean Square	F	*p*
Production rate	17.2691	2	8.635	20.11	0.047
Injection ratio	4.0562	2	2.028	4.723	0.175
Injection temperature	4.0178	2	2.009	4.678	0.176
Error (unassigned column)	0.8588	2	0.4294	—	—

The following significance results are based on the main-effects model, with the unassigned-column mean square used as the error estimate. According to the *p* values of ANOVA results for groundwater drawdown, the influence ranking of each factor on groundwater drawdown is consistent with the results obtained by range analysis. For groundwater drawdown, among the three influencing factors, the injection ratio reached significance at the 95% confidence level. According to the *p* values of the ANOVA results for production temperature, the influence ranking of each factor on production temperature is also consistent with the results of range analysis. For the production temperature, among the three influencing factors, the production rate reached significance at the 95% confidence level.

The operating parameters are also physically interrelated. Production rate and injection ratio jointly determine the reinjection volume and associated hydraulic support, while flow rate influences the advective transport of water injected at different temperatures. The orthogonal analysis quantifies the main effects averaged over the tested combinations. Its significance tests assume that interaction contributions to the unassigned-column variation are sufficiently small; this variation serves as the error estimate rather than a replicated pure-error estimate.

5. Conclusions

A three-dimensional thermo-hydro-mechanical (THM) coupled numerical model was developed to investigate the effects of well spacing, well configurations, and production–injection parameters on the hydraulic and thermal performance of a sandstone geothermal reservoir. The main conclusions are as follows:

(1) Well spacing plays a critical role in balancing groundwater drawdown and thermal interference. After 30 years of operation, a well spacing of 200 m results in a production temperature decline of 2.12 °C, whereas increasing the spacing to 1000 m leads to a groundwater drawdown of 1.62 m. A spacing of 400 m provides a favorable balance between hydraulic and thermal performance, with a groundwater drawdown of approximately 0.5 m and a production temperature decline of only 0.34 °C.

(2) Well configuration significantly influences the hydraulic performance of geothermal reservoirs. Among the 14 configurations investigated, the linear arrangement (Pattern II) exhibits the most favorable performance for both two-injection–one-production and one-injection–two-production systems. In contrast, the diamond-shaped arrangement (Pattern IV) minimizes groundwater drawdown to 0.11 m in the two-injection–two-production system, indicating that the preferred well configuration depends on the production–injection arrangement.

(3) For the sensitivity analysis conducted at a well spacing of 200 m, production–injection parameters exert distinct influences on reservoir hydraulic and thermal responses. The injection ratio is identified as the dominant factor affecting groundwater drawdown (range = 1.53 m, $p = 0.035$), whereas the production rate has the greatest influence on production temperature (range = 3.38 °C, $p = 0.047$). These findings emphasize the importance of coordinating production and injection operations to mitigate groundwater drawdown and thermal interference, thereby supporting the long-term sustainable exploitation of sandstone geothermal reservoirs.

Author Contributions: Conceptualization, Q.S. and Y.Y.; methodology, X.Y. and M.W.; validation, X.Y. and Q.S.; investigation, Y.Y. and M.W.; data curation, Q.S. and P.D.; writing—original draft preparation, M.W.; writing—review and editing, Q.S. and P.D.; visualization, Q.S. and Y.Z.; funding acquisition, M.W. and P.D. All authors have read and agreed to the published version of the manuscript.

Funding: This research has been supported by the Shandong Provincial Research Center of Geothermal Resources and Reinjection (Grant No. LBYKFJJ002), the Dezhou Deep Geological Energy Conservation and Carbon Reduction Key Laboratory (Grant No. LBYKFJJ002), the National Natural Science Foundation Youth Science Fund of China (Grant No. 42307272), and the Innovation Project of Postgraduates in Ningxia University (Grant No. CXXM2026042).

Data Availability Statement: All the data required to evaluate the conclusions of this study are present in the paper. The authors will provide additional data related to this paper upon request.

Conflicts of Interest: The authors declare no conflicts of interest.

References

1. Zhang, G.L.; Liu, S.Q.; Fei, Y.; Li, Y.; Guo, F. Thermo-hydro-mechanical coupling analysis of geothermal reservoirs: Optimizing extraction capacities by revealing influential factors. *Geophys. Eng.* **2024**, *21*, 1040–1055. [CrossRef]
2. Szanyi, J.; Rybach, L.; Abdulhaq, H.A. Geothermal Energy and Its Potential for Critical Metal Extraction-A Review. *Energies* **2023**, *16*, 7168. [CrossRef]
3. Moya, D.; Aldás, C.; Kaparaju, P. Geothermal energy: Power plant technology and direct heat applications. *Renew. Sustain. Energy Rev.* **2018**, *94*, 889–901. [CrossRef]
4. Limberger, J.; Boxem, T.; Pluymaekers, M.; Bruhn, D.; Manzella, A.; Calcagno, P.; Beekman, F.; Cloetingh, S.; Wees, J.D. Geothermal energy in deep aquifers: A global assessment of the resource base for direct heat utilization. *Renew. Sustain. Energy Rev.* **2018**, *82*, 961–975. [CrossRef]
5. Li, H.Y.; Wang, J.F.; Liu, B.; Wang, P.T. Engineering practice of geothermal recharge technology for Leling sandstone thermal storage. *Therm. Sci.* **2023**, *27*, 2525–2536. [CrossRef]
6. Li, J.L.; Kang, F.X.; Qin, P.; Yang, Y.B.; Zheng, T.T.; Chen, T.; Yang, H.T.; Feng, J.G.; Bai, T.; Zhang, L.; et al. Evolution and response mechanism of geo-temperature field in vertically heterogeneous sandstone geothermal reservoirs to reinjection of cooled geothermal water. *Renew. Energy.* **2025**, *252*, 123518. [CrossRef]
7. Subbotina, M.; Mukhina, E.; Karamov, T.; Popov, E.; Kozlova, E.; Morkovkin, A.; Mukhametdinova, A.; Prochukhan, K.; Cheremisin, A. Evolution of reservoir properties of oil shale rocks under hydro-thermal treatment: Investigations from micro- to macro-scale. *Geoenergy Sci. Eng.* **2023**, *228*, 211972. [CrossRef]
8. Yin, H.Y.; Zhou, W.; Dong, F.Y.; Liu, Y.M.; Shi, C.H.; Meng, M.M.; Cheng, W.J. Hydrochemical characteristics and genetic mechanism of porous sandstone geothermal water in northern Jinan, Shandong, China. *Environ. Sci. Pollut. Res.* **2024**, *31*, 24180–24196. [CrossRef]

9. Zheng, T.T.; Axelsson, G.; Kang, F.X.; Zhao, J.C.; Zhang, P.P.; Bai, T.; Yang, X.C.; Zhou, Q.D.; Luo, Y.C. Sustainable geothermal yield through effective reinjection: Reservoir engineering case study of the Dezhou sandstone geothermal reservoir, North Shandong Plain, China. *Geotherm. Energy.* **2025**, *13*, 36. [CrossRef]
10. Azim, R.A.; Alatefi, S.; Aljehani, A. A fully coupled thermo-poroelastic model for energy extraction in naturally fractured geothermal reservoirs: Sensitivity analysis and flow simulation. *Geotherm. Energy.* **2024**, *12*, 26. [CrossRef]
11. Shan, K.; Zou, Q.Q.; Li, C.S.; Yu, Z.W. Dvancements and future prospects in the hydraulic fracturing of geothermal reservoirs. *Energies* **2024**, *17*, 6082. [CrossRef]
12. Li, D.Q.; Li, N.; Jia, J.; Yu, H.G.; Fan, Q.H.; Wang, L.C.; Mohsen, A. Development status and research recommendations for thermal extraction technology in deep hot dry rock reservoirs. *Deep Undergr. Sci. Eng.* **2024**, *3*, 317–325. [CrossRef]
13. Song, G.F.; Li, G.S.; Song, X.Z.; Shi, Y. Multi-objective balanced method of optimizing the heat extraction performance for hot dry rock. *Nat. Gas. Ind. B* **2022**, *9*, 497–510. [CrossRef]
14. Liu, Z.B.; Wu, M.; Zhou, H.Y.; Chen, L.; Wang, X. Performance evaluation of enhanced geothermal systems with intermittent thermal extraction for sustainable energy production. *J. Clean. Prod.* **2024**, *434*, 139954. [CrossRef]
15. Han, D.H.; Xia, Y.; Wang, X.Y.; Ban, F.S.; Li, X.X.; Diao, H.Y.; Guan, Y.Y.; Liu, Y.H.; Fang, F.F.; Zhang, J. Thermo-Hydro-Mechanical Modeling of Geothermal Energy Extraction Using Water and Pressurized CO_2 in Deep Reservoir Systems. *Energies* **2026**, *19*, 3545. [CrossRef]
16. Liu, Z.Z.; Dong, X.; Liu, H.F.; He, Y.H.; Li, S.; Jia, C.; Qin, P.; Li, B.; Ding, P.P. Multi-Field Coupled Numerical Simulation of Geothermal Extraction and Reinjection in the Sandstone Reservoir. *Sustainability* **2025**, *17*, 9646. [CrossRef]
17. Akin, S. Geothermal re-injection performance evaluation using surveillance analysis methods. *Renew. Energy* **2019**, *139*, 635–642. [CrossRef]
18. Wang, Z.; Zhang, C.; Jiang, G.; Wang, Y.; Hu, S. Effect of different exploitation schemes on production performance from the carbonate reservoir: A case study in Xiong'an New Area. *J. Clean. Prod.* **2021**, *314*, 128050. [CrossRef]
19. Liu, L.; Yang, X.; Wang, T.; Ma, P.; Li, Y.; Luo, S.; Zhang, L. Sensitivity-guided thermo-hydro-mechanical modeling and operation of a multi-well geothermal system: A case study in the Xiong'an new area, China. *Case Stud. Therm. Eng.* **2026**, *80*, 107919. [CrossRef]
20. Ling, W.; Liu, Y.X.; Young, R.; Cladouhos, T.T.; Jafarpour, B. Efficient data-driven models for prediction and optimization of geothermal power plant operations. *Geothermics* **2024**, *119*, 102924. [CrossRef]
21. Zhang, Y.J.; Li, C.; Yang, H.; Qu, X. Effects of Well Layout and Injection Rate on Long-Term Heat Extraction Performance in Fractured Geothermal Reservoirs: A DFN-Based Thermo-Hydraulic Study. *Energies* **2026**, *19*, 3115. [CrossRef]
22. Gao, J.Y.; Shi, Q.P. A new mathematical modeling approach for thermal exploration efficiency under different geothermal well layout conditions. *Sci. Rep.* **2021**, *11*, 22930. [CrossRef]
23. Willems, C.J.L.; Nick, H.M. Towards optimisation of geothermal heat recovery: An example from the West Netherlands Basin. *Appl. Energy* **2019**, *247*, 582–593. [CrossRef]
24. Liu, G.; Wang, G.; Zhao, Z.; Ma, F. A new well pattern of cluster-layout for deep geothermal reservoirs: Case study from the Dezhou geothermal field, China. *Renew. Energy* **2020**, *155*, 484–499. [CrossRef]
25. Jiang, H.Y.; Guo, L.L.; Kang, F.X.; Wang, F.G.; Cao, Y.L.; Sun, Z.; Shi, M. Geothermal Characteristics and Productivity Potential of a Super-Thick Shallow Granite-Type Enhanced Geothermal System: A Case Study in Wendeng Geothermal Field, China. *Sustainability* **2023**, *15*, 3551. [CrossRef]
26. Cai, X.L.; Liu, Z.W.; Xu, K.; Li, B.Z.; Zhong, X.; Yang, M.H. Numerical simulation study of an Enhanced Geothermal System with a five-spot pattern horizontal well based onthermal-fluid-solid coupling. *Appl. Therm. Eng.* **2025**, *258*, 124649. [CrossRef]
27. Bujakowski, W.; Tomaszewska, B.; Miecznik, M. The Podhale geothermal reservoir simulation for long-term sustainable production. *Renew. Energy.* **2016**, *99*, 420–430. [CrossRef]
28. Li, J.L.; Kang, F.X.; Bai, T.; Li, Z.H.; Zhao, Q.; Zhang, P.P.; Zheng, T.T.; Sui, H.B. Geo-temperature response to reinjection in sandstone geothermal reservoirs. *Geotherm. Energy* **2023**, *11*, 35. [CrossRef]
29. Sbai, M.A.; Larabi, A. Analyzing the relationship between doublet lifetime and thermal breakthrough at the Dogger geothermal exploitation site in the Paris basin using a coupled mixed-hybrid finite element model. *Geothermics* **2023**, *114*, 102795. [CrossRef]
30. Suilmann, J.; Tischner, T.; Graf, T. Improving geothermal doublet efficiency in multiple sandstone horizons in Hannover/Germany. *Grundwasser* **2025**, *30*, 3–18. [CrossRef]
31. Li, T.Y.; Han, D.X.; Yang, F.S.; Yu, B.; Wang, D.B.; Sun, D.L. Study on the thermal-hydraulic coupling model for the enhanced geothermal systems. In *Computational Science-ICCS 2019*; Rodrigues, J., Cardoso, P., Monteiro, J., Lam, R., Krzhizhanovskaya, V.V., Lees, M.H., Dongarra, J.J., Sloot, P., Eds.; Lecture Notes in Computer Science; Springer: Berlin/Heidelberg, Germany, 2019; Volume 11539, pp. 633–646. [CrossRef]
32. Zhang, W.; Wang, M.J.; Wei, Z.N.; Yu, H.Y.; Wang, C.G.; Wang, D.; Guo, T.K. Study of the fracture propagation and the corresponding heat mining performance of multi-branch radial wells geothermal system based on the THM-D coupling model. *Geoenergy Sci. Eng.* **2024**, *243*, 213302. [CrossRef]

33. Wang, L.C.; Liang, X.; Shi, X.Y.; Han, J.Y.; Chen, Y.; Zhang, W. Heat Transfer Analysis of Enhanced Geothermal System Based on Heat-Fluid-Structure Coupling Model. *Geofluids* **2023**, *8840352*, 1–28. [CrossRef]
34. Ding, Y.; Wei, M.; Liu, R. Parameters of liquid cooling thermal management system effect on the Li-ion battery temperature distribution. *Therm. Sci.* **2021**, *26*, 567–577. [CrossRef]

Disclaimer/Publisher's Note: The statements, opinions and data contained in all publications are solely those of the individual author(s) and contributor(s) and not of MDPI and/or the editor(s). MDPI and/or the editor(s) disclaim responsibility for any injury to people or property resulting from any ideas, methods, instructions or products referred to in the content.